Geophys. J. Int. (1996) **125**, 705–718

An optimal procedure for deriving marine gravity from multi-satellite altimetry

Cheinway Hwang[1] and Barry Parsons[2]

[1] *Department of Civil Engineering, National Chiao Tung University, Hsinchu, Taiwan, ROC*
[2] *Department of Earth Sciences, Oxford University, Oxford, UK*

Accepted 1996 January 8. Received 1996 January 8; in original form 1995 September 4

SUMMARY

An optimal procedure is developed for deriving gravity anomalies from sea-surface height measurements obtained by a number of different satellites, the inclinations of which may vary. We begin by recasting the problem of the conversion of the deflection of the vertical to gravity in the frequency domain. We show that a deterministic approach based on the Vening–Meinesz integral is equivalent in the frequency domain to the stochastically based method of least-squares collocation. A new method for gridding the deflection of the vertical is developed that uses the fact that satellite tracks of the same type (ascending or descending) are nearly parallel, so that values at grid points can be estimated by first performing along-track interpolations, followed by one cross-track interpolation, both using Akima's spline. This gridding method is very efficient compared with methods such as that of fitting minimum curvature surfaces, especially for dense data such as for the 168 day cycles of ERS-1. A weighted least-squares method is then employed to obtain the north and east components of deflection-of-the-vertical components using the gridded along-track components from all of the individual satellite missions. Finally, gravity anomalies are computed from the two deflection-of-the-vertical components in the frequency domain with truncated kernel functions, the use of which is related to the prior removal of a high-degree reference gravity field. This new procedure is more than 100 times faster than least-squares collocation, and yields gravity anomalies with errors that are comparable to those derived by least-squares collocation and smaller than those derived by other recent applications of spectral techniques, as judged by comparisons with ship-gravity measurements. The case of gravity computation for a single altimetric satellite is handled separately, and a method is given to estimate the noise spectra of deflection of the vertical and reduce the numerical problems caused by satellites with high inclination angles. The new procedures make possible quick, yet accurate, global updates of the marine gravity field.

Key words: altimetry, deflection of the vertical, Fourier transforms, gravity anomalies.

INTRODUCTION

Currently there exist altimetric data from five satellite missions, i.e. Geos-3, Seasat, Geosat, ERS-1 and TOPEX/POSEIDON, which may be used for deriving marine gravity. Future altimeter missions will further increase the amount and density of sea-surface height measurements. Consequently, it has become increasingly important to have efficient methods of deriving gravity anomalies from this large amount of altimeter data. The fastest methods have been based on spectral techniques and use of the fast Fourier transform (FFT), and this seems likely to remain the case. Examples of FFT-based methods are those used by Haxby *et al.* (1983), Sandwell (1992), and McAdoo & Marks (1992). As regards the type of data, the use of deflection of the vertical mitigates, to a large extent, problems associated with orbital errors (e.g. Sandwell 1992; Hwang & Parsons 1995). With dense altimeter coverage from several satellites, it will be difficult and time-consuming to make orbital corrections to the sea-surface height measurements to the level required to remove crossover differences and avoid short-wavelength artefacts in the derived gravity field.

If an FFT-based technique is to be used, the immediate problem is that of gridding the measurements. As the number of satellite missions increases, the computer time needed for

gridding the data will become a major burden in the derivation of gravity fields. Furthermore, since deflections of the vertical from different satellite missions have different azimuths, a method for resolving gridded deflections of the vertical with different azimuths into an unique set of north and east components of the deflection of the vertical is an essential step in the derivation of gravity. One method used for this purpose has been described by Sandwell (1984), and has been used in the construction of a global marine gravity field (Sandwell, Yale & Smith 1994).

With these problems as a background, the aim of this study is to develop a fast procedure for deriving marine gravity from multi-satellite altimeter data. The method should also be optimal in terms of a comparison with direct measurements of marine gravity. To this end, we first find a 'best' relationship between deflections of the vertical and gravity anomalies in the frequency domain, considering factors such as the use of a high-degree reference geopotential model and errors in the data. We then look at an efficient gridding technique that exploits the characteristics of altimetry data distribution and avoids unnecessary assumptions. The issue of combining deflections of the vertical with different inclinations is investigated, and we present a method of obtaining the north and east components of the deflection of the vertical using a weighted least-squares. As an illustration of the ways of estimating data noise and dealing with the problems caused by high inclination angles, we also look at the case of a single satellite. Finally we evaluate these procedures for converting deflections of the vertical to gravity by comparing the satellite-derived gravity anomalies with ship gravity; gravity anomalies derived by the method of least-squares collocation, and those obtained by Sandwell *et al.* (1994) are assessed in the same way. Tests of the steps in our new procedure have been carried out for two areas: the area around the Reykjanes Ridge, defined by $50° < \phi < 65°$, $320° < \lambda < 340°$; and an area in the South Pacific defined by $-25° < \phi < -10°$, $230° < \lambda < 250°$, where ϕ is the latitude and λ is the longitude.

GRAVITY TO DEFLECTION-OF-THE-VERTICAL CONVERSION: DUALITY OF DETERMINISTIC AND STOCHASTIC APPROACHES IN THE FREQUENCY DOMAIN

To use an FFT-based method to derive gravity from deflections of the vertical, we first have to find the relationship between the gravity anomaly and deflection of the vertical in the frequency domain. Such a relationship can be established using either a deterministic approach or a stochastic approach. For the deterministic approach, we first express the gravity anomaly and deflections of the vertical as functionals of the Earth's disturbing potential, T, specifically:

$$\Delta g = -\frac{\partial T}{\partial z} - 2\frac{T}{R_e} \approx -\frac{\partial T}{\partial z}, \tag{1}$$

$$\xi = -\frac{1}{\gamma}\frac{\partial T}{\partial y} = -\frac{1}{\gamma R_e}\frac{\partial T}{\partial \phi}, \tag{2}$$

$$\eta = -\frac{1}{\gamma}\frac{\partial T}{\partial x} = -\frac{1}{\gamma R_e \cos\phi}\frac{\partial T}{\partial \lambda}, \tag{3}$$

where Δg is the gravity anomaly, ξ and η are the north and east components of the deflection of the vertical, respectively, γ is the normal gravity on the reference ellipsoid, x, y, z are the local rectangular coordinates (x positive to the east, y positive to the north and z positive upwards), and R_e is the Earth's mean radius (≈ 6371 km). The approximation in (1) can be made if we use a remove/restore procedure in which the long-wavelength components are removed from the data (see below). The relationship between geoidal undulation and gravity anomaly in the planar approximation is given by Stokes' formula (see Schwarz, Sideris & Forsberg 1990):

$$N(x_p, y_p) = \frac{1}{2\pi\gamma}\int\int_E \frac{\Delta g(x, y)}{\sqrt{(x-x_p)^2 + (y-y_p)^2}}\,dx\,dy = \frac{1}{2\pi\gamma}\Delta g * \frac{1}{r}, \tag{4}$$

where $*$ is the convolution operator, E is the domain of integration in the XY-plane, and $r = \sqrt{x^2 + y^2}$. Using Bruns' formula, $N = T/\gamma$, and eqs (2)–(4), we obtain the Vening–Meinesz integral:

$$\begin{Bmatrix}\xi(x_p, y_p)\\ \eta(x_p, y_p)\end{Bmatrix} = \frac{1}{2\pi\gamma}\int\int_E \frac{\Delta g(x, y)}{[(x-x_p)^2 + (y-y_p)^2]^{3/2}}\begin{Bmatrix}y-y_p\\ x-x_p\end{Bmatrix}dx\,dy$$

$$= \frac{1}{2\pi\gamma}\Delta g * \begin{Bmatrix}l_\xi\\ l_\eta\end{Bmatrix}. \tag{5}$$

It is clear from (5) that the kernel functions of ξ and η are

$$\begin{Bmatrix}l_\xi\\ l_\eta\end{Bmatrix} = \frac{1}{r^3}\begin{Bmatrix}y\\ x\end{Bmatrix}. \tag{6}$$

Noting that the form of the Fourier transform used here is given by

$$F(u, v) = \int_{-\infty}^{\infty}\int_{-\infty}^{\infty} f(x, y)\exp[-i2\pi(ux + vy)]\,dx\,dy, \tag{7}$$

on transforming eq. (5) we obtain

$$\begin{Bmatrix}\Xi(u, v)\\ H(u, v)\end{Bmatrix} = \frac{-i}{\gamma q}\Delta G(u, v)\begin{Bmatrix}v\\ u\end{Bmatrix}, \tag{8}$$

where $q = \sqrt{u^2 + v^2}$ is the circular frequency. Thus, in theory, it is possible to determine the gravity anomaly by knowing only either ξ or η. In satellite altimetry, however, we obtain both the north and east components of the deflection of the vertical by resolving the ascending and descending along-track components (see below), and we wish to use them in an optimal way. In this case we have two observations, Ξ and H, and one unknown, ΔG, and hence each entry of (8) forms an observation equation. Assuming that the weights for Ξ and H are identical, we can derive a unique ΔG from Ξ and H by making use of the least-squares principle (see, for example, Koch 1987):

$$\Delta G(u, v) = \frac{i\gamma}{q}(uH + v\Xi). \tag{9}$$

Eq. (9) is identical to the formulae given in Sandwell (1992) and McAdoo & Marks (1992), who derived their formulae using Laplace's equation and downward continuation. Approaches that use either (8) or (9) are deterministic in nature.

In the stochastic approach, the prediction of the gravity anomaly from deflections of the vertical may be accomplished by least-squares collocation (e.g. Hwang & Parsons 1995). Following Moritz (1980), the general prediction formula of

least-squares collocation involving two types of data reads

$$s = C_{sl} C_{ll}^{-1} l = (C_1 C_2) \begin{pmatrix} C_{11} C_{12} \\ C_{21} C_{22} \end{pmatrix}^{-1} \begin{pmatrix} l_1 \\ l_2 \end{pmatrix}, \tag{10}$$

where s denotes the vector containing the signal, l_1 and l_2 are two vectors containing observations of type 1 and type 2, C_i is the covariance function between s and data of type i, and C_{ij} are the covariance functions among the data. Assuming observations are available for the entire XY-plane, the right-hand side of (10) can be viewed as the convolution between kernel functions f_1, f_2 and the data contained in l_1, l_2, namely

$$s = f_1 * l_1 + f_2 * l_2, \tag{11}$$

where

$$(f_1 f_2) = (C_1 C_2) \begin{pmatrix} C_{11} C_{12} \\ C_{21} C_{22} \end{pmatrix}^{-1}. \tag{12}$$

The Fourier transform (FT) of (11) is

$$S = F_1 L_1 + F_2 L_2. \tag{13}$$

This is equivalent to a system identification problem where the spectra F_1 and F_2 are to be identified (Bendat & Piersol 1993). Fourier transforming (12) and using the fact that the covariance function and spectral density function form a Fourier transform pair gives

$$\begin{pmatrix} F_1 \\ F_2 \end{pmatrix} = \begin{pmatrix} G_{11} G_{12} \\ G_{21} G_{22} \end{pmatrix}^{-1} \begin{pmatrix} G_1 \\ G_2 \end{pmatrix}, \tag{14}$$

where G_{ij} are the auto- or cross-spectral density functions of l_1 and l_2, and G_i is the cross-spectral density function between l_i and s, namely

$$G_{ij} = \lim_{T_x, T_y \to \infty} \frac{1}{T_x T_y} L_i^* L_j, \tag{15}$$

$$G_i = \lim_{T_x, T_y \to \infty} \frac{1}{T_x T_y} L_i^* S, \tag{16}$$

with T_x, T_y being the record lengths in the X, Y directions, respectively. Note that the above definitions have been adopted from Bendat & Piersol (1993), and here the symbol '*' represents the conjugate operator. If the two vectors l_1 and l_2 are linearly correlated, which is true for the north and east deflection of the vertical components (see eq. 8), we obtain (see Vassiliou 1986)

$$F_1 = \frac{G_1}{G_{11} + G_{22}}, \qquad F_2 = \frac{G_2}{G_{11} + G_{22}}. \tag{17}$$

Now, let s be a vector containing gravity anomalies, and l_1 and l_2 be vectors containing ξ and η, respectively. By the differentiation theorem of FT we have, with (1)–(3),

$$\begin{aligned} \Delta G(u, v) &= -\frac{\partial}{\partial z} T(u, v, z)\Big|_{z=0} = -\frac{\partial}{\partial z} [T(u, v)\, \mathrm{e}^{-2\pi q z}]\Big|_{z=0} \\ &= 2\pi q T(u, v), \\ \Xi(u, v) &= -\frac{i}{\gamma} 2\pi v T(u, v), \\ H(u, v) &= -\frac{i}{\gamma} 2\pi u T(u, v), \end{aligned} \tag{18}$$

then,

$$\begin{aligned} G_{11} &= \frac{1}{\gamma^2} 4\pi^2 v^2 S_{\mathrm{T}}, \\ G_{22} &= \frac{1}{\gamma^2} 4\pi^2 u^2 S_{\mathrm{T}}, \\ G_1 &= \frac{iq}{\gamma} 4\pi^2 v S_{\mathrm{T}}, \\ G_2 &= \frac{iq}{\gamma} 4\pi^2 u S_{\mathrm{T}}, \end{aligned} \tag{19}$$

where S_{T} is the spectral density function of the Earth's disturbing potential. Therefore, with (17) we have

$$F_1 = \frac{iyv}{q}, \qquad F_2 = \frac{iyu}{q}. \tag{20}$$

Substituting F_1 and F_2 into (13), we obtain (9). This shows that in the frequency domain the deterministic approach based on the Vening–Meinesz integral, and the stochastic approach based on least-squares collocation yield the same relationship between the gravity anomaly and the two deflection of the vertical components. The implication is that when using (9) for transformation of deflections of the vertical into gravity, the property of minimum-error variance of the predicted gravity anomalies, which is intrinsic to least-squares collocation, is preserved (*cf.* Moritz 1980).

FAST GRIDDING BY SPLINES

To use the frequency-domain approach, the first step is to grid the ascending and descending deflection of the vertical from individual satellites. Packages such as GMT (Wessel & Smith 1991) and IMSL contain programs for gridding. However, they are designed for general purposes and do not take advantage of the characteristics of altimetry data distributions. Furthermore, the ascending and descending deflections of the vertical are in fact functions of three variables—latitude, longitude and azimuth. Therefore, if the gridding is done with a 2-D interpolant, the resulting value is in some sense a weighted mean of the deflections of the vertical surrounding the grid points, ignoring the fact that the deflections of the vertical used have different azimuths. If the area searched is small, this will not create a serious problem since the variation of azimuth in this case will be small. To avoid the constant-azimuth assumption, we can view the along-track deflection of the vertical as a function of along-track distance. The azimuth is implicitly contained in the distance variable as

$$\varepsilon(s) = \varepsilon(s(\alpha)), \tag{21}$$

where ε is deflection of the vertical, s is along-track distance and α is azimuth. We can also treat the cross-track deflection of the vertical as a function of cross-track distance.

A fast algorithm for gridding the along-track deflection of the vertical can be based on these simple considerations. It is known that, over a short interval of time, a satellite's motion is governed by secular variations in the six Keplerian elements (Kaula 1966). Thus, within a small latitudinal band, ground tracks of the same type (ascending or descending) are almost

parallel and we may fit a straight line to each of the ground tracks by least-squares. These lines help the search for the intersection points described below. As shown in Fig. 1, at any given grid point P, we first find the intersection point between the first track to the left and a line passing through P and perpendicular to this track, so that the distance from P to the track is a minimum. From (21), the deflection of the vertical at this intersection point can be interpolated from the deflections of the vertical along the same track. We then proceed to the second track to the left, and interpolate the deflection of the vertical on to a point whose distance to the first intersection point is a minimum. The process is repeated for a specified number of tracks to the left. For tracks on the right side of P, the method of obtaining the along-track deflection of the vertical is the same. When interpolating the along-track deflection of the vertical we also record the cross-track distances to P, negative for the tracks to the left and positive for the tracks to the right. Finally we perform a cross-track interpolation using the recorded deflections of the vertical and cross-track distances to obtain the deflection of the vertical at the grid point P.

Many schemes were tested for the along- and cross-track interpolations. Owing to the unequally spaced knots, methods such as the natural cubic spline and Lagrange's polynomials create very large oscillations on some occasions, and the deflections of the vertical are corrupted by artefacts in places. We found that Akima's spline (de Boor 1978), which was designed to combat large oscillations, works well in this application. Furthermore, we suggest that at most three tracks to the left and to the right—a total of six—are sufficient, and that the distances from P to the leftmost or the rightmost track should not exceed three times the average cross-track spacing. For each along-track interpolation, the data distances to the intersection point should not exceed 21 km.

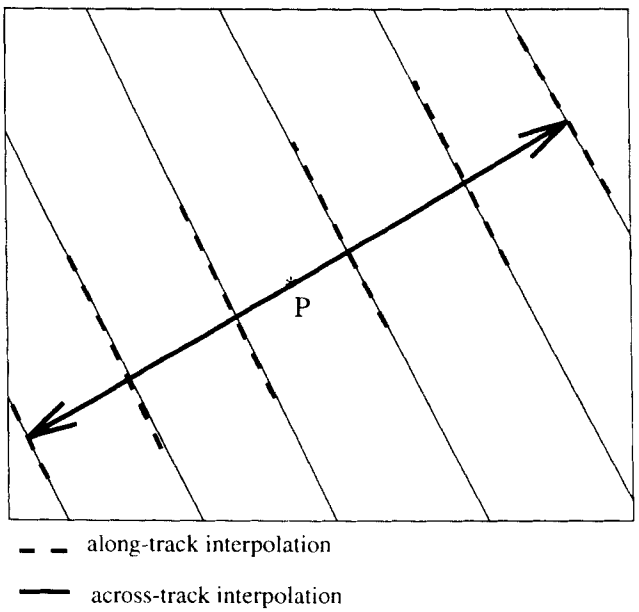

Figure 1. Sketch showing the gridding of deflections of the vertical by splines. The gridding is first carried out by along-track interpolations on the two sides of point P (directions along dashed lines), followed by one cross-track interpolation (direction along the solid line).

Fig. 2 compares ERS-1/35-day deflections of the vertical gridded by the routine 'surface' in GMT (Wessel & Smith 1991)—this is based on fitting a minimum-curvature surface (Smith & Wessel 1990)—and the program 'spgrid', which is based on the method just described. The minimum-curvature method tends to break up features that are clearly linear. Since only a few data points are used at each grid point, the new method is also very efficient, especially for very dense data. Using ERS-1/168-day data over the Reykjanes Ridge, with a grid spacing of $3' \times 3'$, 'surface' needed 272 CPU seconds on a Sparc10 M41 computer, compared with 43 seconds for 'spgrid'.

The new method also provides weights to be associated with the interpolated deflection of the vertical. Based on the error estimate for Akima's spline (de Boor 1978), the weight, p, at a grid is taken to be

$$p = \frac{1}{\sigma_x^2 + \sigma_l^2 + \sigma_r^2}, \tag{22}$$

where σ_x^2 is the unscaled error variance associated with the cross-track interpolation, σ_l^2 is the unscaled error variance associated with the along-track interpolation at the first track to the left and σ_r^2 is the same as σ_l^2, but to the right. Each of the unscaled error variances is determined by

$$\sigma_i^2 = x_1^2 x_2^2, \tag{23}$$

where x_1 and x_2 are the distances from an intersection point (or P) to the data points before and after this point (or P). The weight p serves as a measure of the 'importance' of a gridded deflection of the vertical, and is used in the least-squares estimation of the north and east components of the deflection of the vertical described below.

LEAST-SQUARES ESTIMATION OF NORTH AND EAST DEFLECTIONS OF THE VERTICAL FROM MULTI-SATELLITE DATA

Having gridded the along-track deflections of the vertical, the next step is to resolve the north and east components of the deflection of the vertical. First, consider the case of one satellite. As shown in Fig. 3, the deflection of the vertical along an ascending track, ε_a, and the deflection of the vertical along a descending track, ε_d, may be obtained by numerically differentiating two successive along-track sea-surface heights (Hwang & Parsons 1995). The relationship between the component of the deflection of the vertical along an arbitrary azimuth α and the north and east components ξ and η can be expressed as (Heiskanen & Mortiz 1985)

$$\varepsilon = \xi \cos\alpha + \eta \sin\alpha. \tag{24}$$

The approximate azimuth of an along-track deflection of the vertical can be determined by the formulae given by Sandwell (1992) or Hwang & Parsons (1995). At the crossover of two satellite ground tracks, the relationship between the azimuth of the ascending track, α_a, and that of the descending track, α_d, is (Sandwell 1992)

$$\alpha_d = \pi - \alpha_a. \tag{25}$$

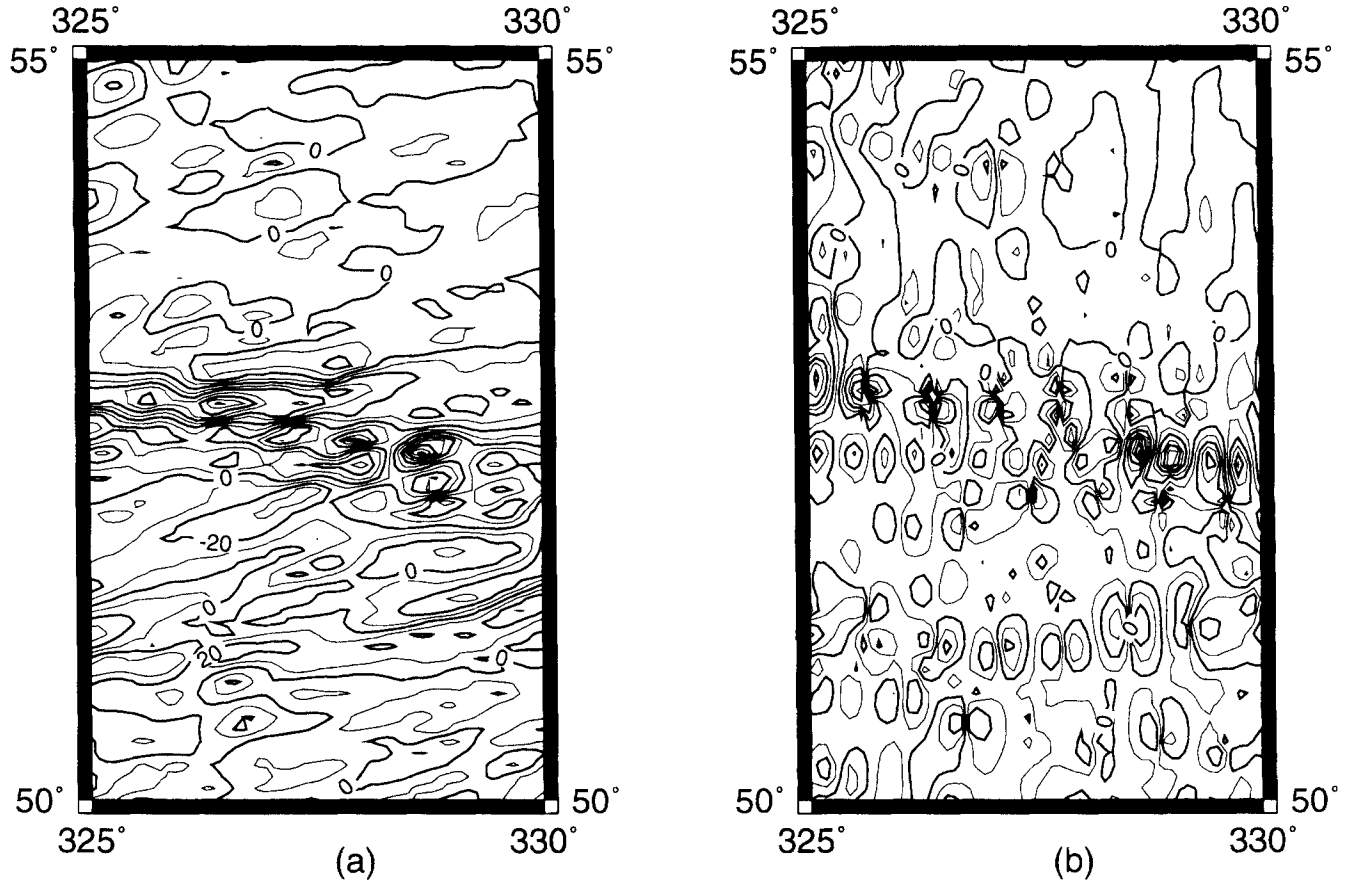

Figure 2. Comparison of ERS-1/35-day ascending deflection of the vertical over Gibb's Fracture Zone, gridded by program 'spgrid' (a), and by program 'surface' (b). Owing to the large cross-track spacing, the deflection of the vertical by 'surface' contains artefacts, which are not found in the deflection of the vertical by 'spgrid'.

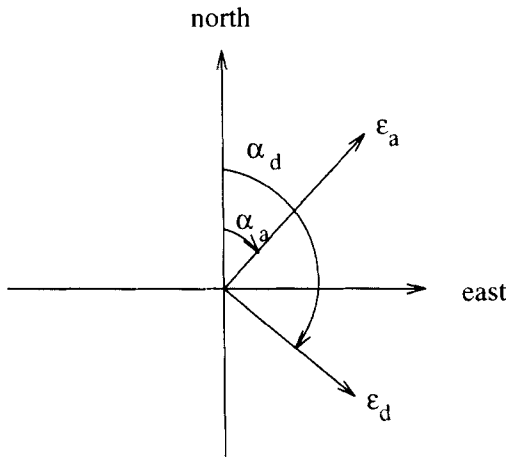

Figure 3. The azimuth (a_a) of an ascending deflection of the vertical (ε_a), and the azimuth (a_d) of a descending deflection of the vertical (ε_d) at a crossover of two satellite ground tracks.

Therefore, for the components of the deflection of the vertical along the ascending (ε_a) and descending (ε_d) tracks we have

$$\begin{aligned}\varepsilon_a &= \xi \cos \alpha_a + \eta \sin \alpha_a ,\\ \varepsilon_d &= \xi \cos \alpha_d + \eta \sin \alpha_d = -\xi \cos \alpha_a + \eta \sin \alpha_a .\end{aligned} \tag{26}$$

Thus we can obtain ξ and η from the ascending and the descending deflection of the vertical as

$$\begin{aligned}\xi &= \frac{1}{2 \cos \alpha_a}(\varepsilon_a - \varepsilon_d),\\ \eta &= \frac{1}{2 \sin \alpha_a}(\varepsilon_a + \varepsilon_d).\end{aligned} \tag{27}$$

If the inclination of the satellite's oribital plane is nearly 90°, or the work area is over the area where the satellite reaches its extreme latitudes, the use of the above algorithm will yield numerical problems. This case is treated in Appendix A.

Now consider the case of multiple satellites, the inclinations of which will, in general, differ. Assume that we have n sets of along-track deflections of the vertical at a given grid point, each set containing both ascending and descending deflections of the vertical. We seek a solution for the north and east components of the deflection of the vertical from the n sets of observations. For $n > 1$, this forms a typical adjustment problem for which we can write the observation equations as

$$\begin{aligned}\varepsilon_a^i + v_a^i &= \xi \cos \alpha_a^i + \eta \sin \alpha_a^i ,\\ \varepsilon_d^i + v_d^i &= -\xi \cos \alpha_a^i + \eta \sin \alpha_a^i ,\\ i &= 1, 2, \ldots, n ,\end{aligned} \tag{28}$$

where v_a^i and v_d^i are the residuals of the ascending and

descending components, respectively, of the deflection of the vertical for set i. Written in matrix form, eq. (28) reads

$$\mathbf{V}+\mathbf{L}=\mathbf{AX}, \qquad \mathbf{\Sigma}_{\mathrm{L}}=\sigma_0^2\mathbf{P}^{-1}, \tag{29}$$

where vector $\mathbf{V}$ contains the residuals, $\mathbf{L}$ contains the observations, $\mathbf{A}$ is the design matrix, $\mathbf{X}$ contains the unknowns ξ, η, $\mathbf{P}$ is the weight matrix and σ_0^2 is the variance of unit weight. $\mathbf{P}$ will be a diagonal matrix if all the deflections of the vertical are uncorrelated. The least-squares solution of (29) is

$$\mathbf{X}=\mathbf{N}^{-1}\mathbf{U}, \tag{30}$$

where $\mathbf{N}=\mathbf{A}^{\mathrm{T}}\mathbf{PA}$, $\mathbf{U}=\mathbf{A}^{\mathrm{T}}\mathbf{PL}$. Furthermore, if we write

$$\mathbf{N}=\begin{pmatrix} a & b \\ b & c \end{pmatrix}, \qquad \mathbf{U}=\begin{pmatrix} t \\ s \end{pmatrix}, \tag{31}$$

then these matrix elements can be analytically expressed as

$$\begin{aligned} a &= \sum_{i=1}^{n} (\cos\alpha_{\mathrm{a}}^i)^2(p_{\mathrm{a}}^i+p_{\mathrm{d}}^i), \\ b &= \sum_{i=1}^{n} \cos\alpha_{\mathrm{a}}^i \sin\alpha_{\mathrm{a}}^i(p_{\mathrm{a}}^i-p_{\mathrm{d}}^i), \\ c &= \sum_{i=1}^{n} (\sin\alpha_{\mathrm{a}}^i)^2(p_{\mathrm{a}}^i+p_{\mathrm{d}}^i), \\ t &= \sum_{i=1}^{n} \cos\alpha_{\mathrm{a}}^i(p_{\mathrm{a}}^i\varepsilon_{\mathrm{a}}^i-p_{\mathrm{d}}^i\varepsilon_{\mathrm{d}}^i), \\ s &= \sum_{i=1}^{n} \sin\alpha_{\mathrm{a}}^i(p_{\mathrm{a}}^i\varepsilon_{\mathrm{a}}^i+p_{\mathrm{d}}^i\varepsilon_{\mathrm{d}}^i), \end{aligned} \tag{32}$$

where p_{a}^i and p_{d}^i are the weights of the ascending and descending deflection of the vertical, respectively. The weights of deflection of the vertical play a crucial role in obtaining reliable estimates of ξ and η. In estimation theory, the weight of an observation is normally taken as the inverse of its error variance. The error in gridded deflections of the vertical contains two parts: that arising from the interpolation; and the error in the original along-track components of the deflection of the vertical. The former will be termed the interpolation error and the latter, the commission error. The interpolation error can be obtained only if we know the variance of unit weight, $\hat{\sigma}_0^2$, associated with the weight given in (22). To estimate this we first assume that the deflections of the vertical contain only interpolation errors, and hence the weights required in (32) will be just given by those in (22). On this assumption, we obtain a solution of the normal eqs (30), and calculate the vector $\mathbf{V}$, leading to the estimate

$$\hat{\sigma}_0^2=\frac{\mathbf{V}^{\mathrm{T}}\mathbf{PV}}{n-2}. \tag{33}$$

With $\hat{\sigma}_0^2$, the estimate of the interpolation error is

$$\sigma_{\mathrm{I}}^2=\frac{\hat{\sigma}_0^2}{p}. \tag{34}$$

Finally the total error is given by

$$\sigma_{\mathrm{t}}^2=\sigma_{\mathrm{I}}^2+\sigma_{\mathrm{c}}^2, \tag{35}$$

where σ_{c} is the commission error. The estimation of ξ and η is then repeated using (30), but with the new data weight of $1/\sigma_{\mathrm{t}}^2$. Based on the work by Hwang & Parsons (1995), and comparisons between the satellite-derived gravity and ship gravity, a good choice for the deflection-of-the-vertical commission errors of Seasat, Geosat/ERM (average over up to 60 cycles), Geosat/GM, ERS-1/35-day (average over 18 cycles), ERS-1/168-day and TOPEX/POSEIDON (average over first 36 cycles) are 10.0, 0.97, 10.0, 1.88, 10.0 and 2.03 μrad, respectively. With the new data weight a refined estimate of the variance of unit weight can be obtained, again using (33). The error variances of the estimated ξ and η are the diagonal elements of the matrix $\hat{\sigma}_0^2\mathbf{N}^{-1}$. Note that at grid nodes near land or isolated bodies it is sometimes impossible to obtain the two components due to lack of data, as indicated by the zero determinants of the normal matrices. To avoid discontinuity and edge effect, we fill the empty nodes using the weighted means from nearby non-empty nodes when the entire grid is established.

FORMULA IN THE CASE OF A HIGH-DEGREE REFERENCE FIELD

The deflection of the vertical to gravity conversion formulae must next be modified in the case when a remove/restore procedure is used. In such a procedure, reference values computed from a geopotential model are removed from the observations, and the residual observations used as input to the conversion formulae such as (9). There are two issues related to this procedure. One concerns the optimal maximum spherical harmonic degree to be used, and the other the modification of the kernel functions. In the first case, we adopt the suggestion of Wang (1993), who recommended the use of the highest degree available in the chosen geopotential model, provided that the geopotential coefficients were properly scaled. Specifically, in the case of the conversion of deflection of the vertical to gravity, the reference components of the deflection of the vertical and the reference values of gravity should be computed by

$$\xi^{\mathrm{ref}}=\sum_{n=2}^{Nmax}\xi_n S_n, \tag{36}$$

$$\eta^{\mathrm{ref}}=\sum_{n=2}^{Nmax}\eta_n S_n, \tag{37}$$

$$\Delta g^{\mathrm{ref}}=\sum_{n=2}^{Nmax}\Delta g_n S_n, \tag{38}$$

where ξ_n, η_n and Δg_n are the degree n terms in spherical harmonic expansions for the north and east components of the deflection of the vertical, and of the gravity anomaly, respectively, and $Nmax$ is the maximum expansion degree. The scaling factor, S_n, which minimizes the effect of coefficient errors and the truncation error due to the finite support of a data domain, was given by Wang (1993) as

$$S_n=\frac{c_n}{c_n+\varepsilon_n}, \tag{39}$$

where c_n and ε_n are the degree variance and error degree variance of the Earth's anomalous potential implied by the chosen reference field. Fig. 4 shows the S_n values as computed from the OSU91A model (Rapp, Wang & Pavlis 1991), which is the reference model used in this study.

The second issue is closely related to the first one. Owing to the use of a high-degree field, as suggested above, the long- and medium-wavelength components of the deflection of the vertical will be removed, and hence the residual gravity anomaly at a computation point is effectively the result of the convolution of the kernel functions and the residual deflection

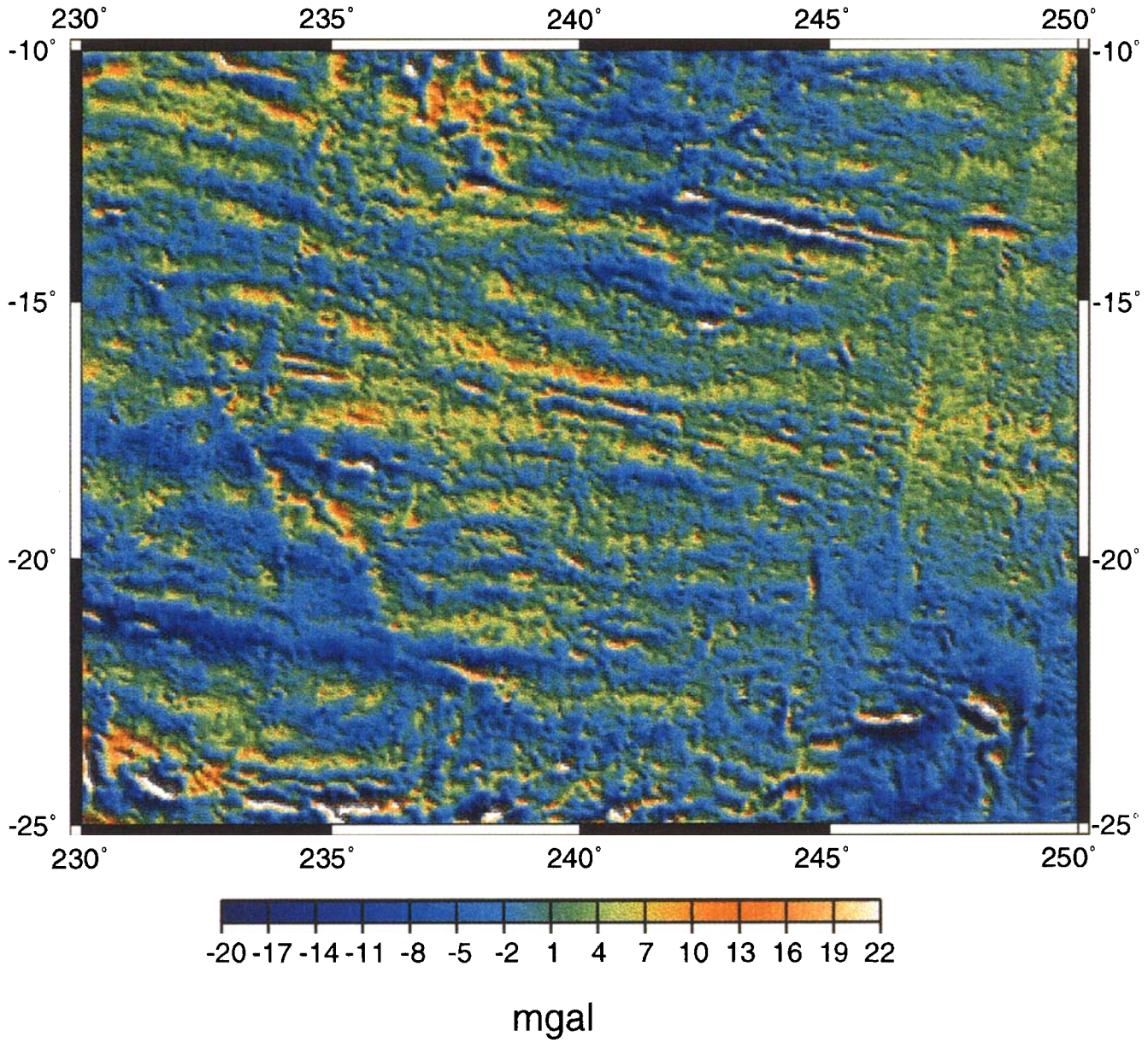

Figure 6. A shaded-relief colour map of the satellite-derived gravity anomalies over the South Pacific.

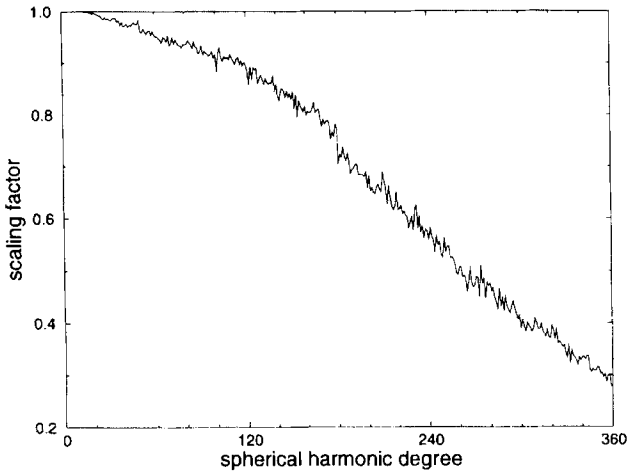

Figure 4. Scaling factors S_n of OSU91A geopotential coefficients for minimizing coefficient errors and truncation error.

of the vertical within a spherical cap of a short radius centred at this point. This observation is reflected in the use of a small inversion cell in least-squares collocation (e.g. Hwang & Parsons 1995). The same principle can be applied in the FFT-based method, through the modification of the kernel functions in (6), rather than of the data domain as in least-squares collocation. Specifically, using a spherical cap of radius R, the truncated kernel functions for the transformation of deflections of the vertical into gravity, obtained by modifying the kernels in (6), are

$$\begin{Bmatrix} \bar{l}_\xi \\ \bar{l}_\eta \end{Bmatrix} = \begin{Bmatrix} l_\xi \\ l_\eta \end{Bmatrix} w(x, y), \tag{40}$$

where

$$w(x, y) = \begin{cases} 1, & r = \sqrt{x^2 + y^2} \le R, \\ 0, & r > R. \end{cases} \tag{41}$$

The FT of $\bar{l}_\xi$ and $\bar{l}_\eta$ can be computed either numerically or analytically. Analytical formulae using Fourier series for the FT of $\bar{l}_\xi$ and $\bar{l}_\eta$ are given in Appendix B. Based on the tests made in Appendix B, we recommend the use of the analytical formulae in (B13) to compute the FT of the truncated kernels. One may be concerned with the potential problem that, in (41), side lobes of the spectrum of $w(x, y)$ will distort the high-frequency parts of the spectra of the truncated kernels. In fact this problem does not occur, since the kernel functions l_ξ, l_η decay rapidly, and the spectra of the truncated kernels derived in Appendix B vary smoothly.

Using the truncated kernels, the relationships between the north and east components of the deflection of the vertical and the gravity anomaly, in the frequency domain, are

$$\begin{Bmatrix} \Xi(u, v) \\ H(u, v) \end{Bmatrix} = \frac{1}{2\pi\gamma} \Delta G(u, v) \begin{Bmatrix} \bar{L}_\xi(u, v) \\ \bar{L}_\eta(u, v) \end{Bmatrix}. \tag{42}$$

Furthermore, since $\bar{L}_\xi$ and $\bar{L}_\eta$ contain only imaginary parts, we can write

$$\bar{L}_\xi(u, v) = iR_\xi(u, v) = iR_\eta(v, u) = \bar{L}_\eta(v, u). \tag{43}$$

Using the least-squares method as for deriving (9), a unique solution of the spectrum of gravity anomaly is

$$\Delta G(u, v) = i2\pi\gamma \frac{R_\xi \Xi(u, v) + R_\eta H(u, v)}{R_\xi^2 + R_\eta^2}. \tag{44}$$

Furthermore, we can anticipate that the errors in the estimates of the north and east components of the deflection of the vertical will be different. The difference in accuracy will be particularly pronounced if altimetric data from satellites with very high or low inclinations, such as ERS-1, dominate the solution in (30) (see the discussion in Appendix A). For example, using Seasat, Geosat/ERM, ERS-1/35-day, and ERS-1/168-day data over the Reykjanes Ridge, it was found that the north and east deflection of the vertical components have average errors of 1.79 and 4.19 μrad respectively. Over the South Pacific the corresponding numbers are 1.51 and 5.49 μrad. Because of the difference in errors in the north and east components of the deflection of the vertical, we should further refine (44), taking into account the estimated deflection of the vertical errors. The effect of these errors is two-fold. First, assuming that the estimated deflections of the vertical contain only white noise, and that the spectra of the white noises are those corresponding to the averaged error variances, we can derive the Gaussian-fitted Wiener filters for the north and east components of the deflection of the vertical, using the same approach as in Appendix A [see (A17)–(A20)]. Second, the average error variances can serve as weights in estimating the gravity-anomaly spectrum, so that instead of eq. (44), we use

$$\Delta G(u, v) = i2\pi\gamma \frac{P_\xi R_\xi \tilde{\Xi}(u, v) + P_\eta R_\eta \tilde{H}(u, v)}{P_\xi R_\xi^2 + P_\eta R_\eta^2}, \tag{45}$$

where P_ξ and P_η are the inverses of the averaged error variances of the estimated north and east deflection of the vertical components, respectively, and $\tilde{\Xi}$ and $\tilde{H}$ are the filtered north and east deflection of the vertical components, respectively. Using Seasat, Geosat/ERM, ERS-1/35-day, and ERS-1/168-day data, it was found that the filter widths of the Gaussian-fitted Wiener filters for the north and east components over the Reykjanes Ridge are 6.04 and 6.91 km, respectively, and over the South Pacific the corresponding numbers are 6.40 and 6.99 km. The filter widths of the east component in the two test areas are larger than the widths of the north component, and this is consistent with the fact that the east component has a larger noise level than the north component.

GRAVITY ANOMALIES FROM MULTI-SATELLITE ALTIMETRY

Summarizing the above developments, the procedure for deriving marine gravity anomalies from multi-satellite altimetry is

(1) grid along-track component of the deflection of the vertical for ascending and descending tracks for each satellite;

(2) at each grid point, estimate the north and east deflection-of-the-vertical components by least-squares using ascending and descending tracks from all satellites;

(3) Fourier transform the north and east components of the deflection of the vertical and filter separately using Wiener filters;

(4) use the filtered components of the deflection of the

Table 1. Standard deviations of the differences (in mgal) between ship gravity and satellite gravities derived using various formulae.

formula	Reykjanes Ridge	South Pacific
equation (9)	8.38	4.85
equation (44)	8.21	4.74
equation (45), but with $S_n = 1$ for all n	7.22	4.02
equation (45)	7.05	3.94

vertical to calculate the spectrum of gravity anomaly with (45) and then do an inverse FFT.

Regarding the last step, we have presented three different formulae for converting deflection of the vertical to gravity anomaly, evolving from (9) to (44), then to (45). In Table 1 we evaluated the results from using the three formulae, and it is concluded that (45) is the best. The cap size R in (41) is set to 1°, based on the experience of Hwang & Parsons (1995), who used a cell size of 0.5° plus 0.25° data border in their least-squares collocation computations. In fact, any values for R between 0.75° and 2° will yield similar results. However, if R is too large, for example $R = 3°$ or larger, the rms difference between the satellite gravity and the ship gravity increases. For the reasons discussed earlier, we chose to use the scaled OSU91A geopotential model to degree 360 as the reference field. In Table 1 we also list the result when the OSU91A coefficients are not scaled. This choice produces a slightly worse result than using the scaled coefficients (see the last two rows in Table 1). The effect of the flat-earth approximation in FFT is negligible (Sideris & Li 1993). Finally, since edge effect is inevitable in FFT unless one uses 100 per cent padding, we recommend that gridded values within 1° of the grid borders are not used. Maps of gravity anomalies on a 3′ × 3′ grid for the two test areas, around the Reykjanes Ridge and in the South Pacific, are shown in Figs 5 and 6.

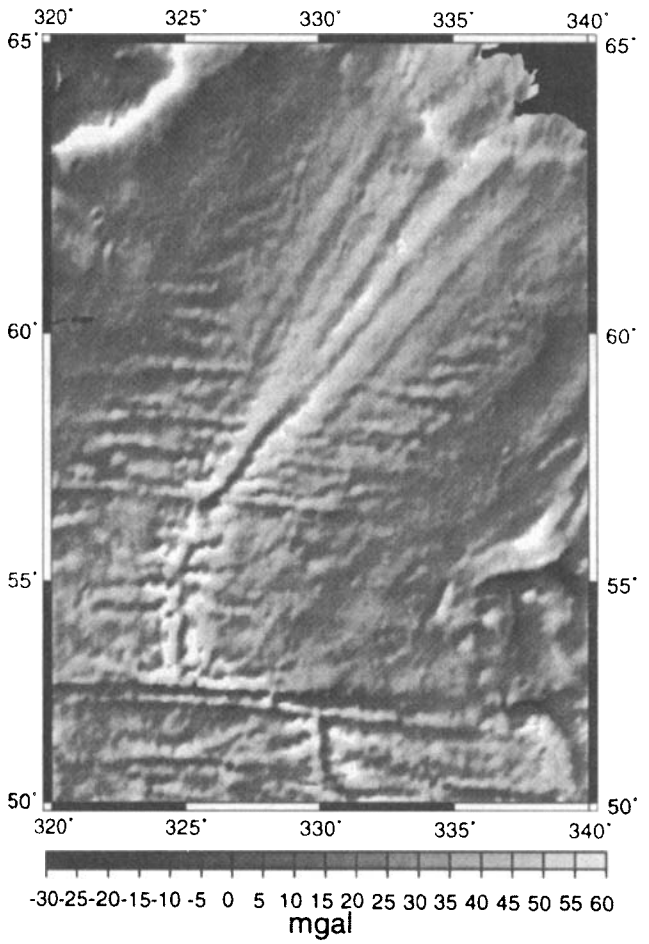

Figure 5. A grey-shaded map of the satellite-derived gravity anomalies over the Reykjanes Ridge.

DISCUSSION

Table 2 shows the differences among the ship gravity and the satellite gravity derived with the above procedure, gravity derived by least-squares collocation as in Hwang & Parsons (1995), and gravity derived by Sandwell *et al.* (1994), for the Reykjanes Ridge and the South Pacific areas. For the three satellite gravity fields in Table 2, the data used are from Seasat, Geosat/ERM ERS-1/35-day and ERS-/168-day. Geosat/GM data could not be used because Geosat/GM data north of 30°S were recently declassified (Carlowicz 1995), but were not available to the authors. It is noted that, due to high latitudes, the density of the altimeter data over the Reykjanes Ridge is relatively high compared with that over the South Pacific area. Also, before comparisons were made, the long-wavelength deviations between satellite-derived gravity and ship gravity were removed, as described in Hwang & Parsons (1995). In all cases, least-squares collocation gives the smallest rms differences from the ship gravity, followed by the procedure described in this paper. The computing times required by these two methods on a Sparc10 M41 computer are also given in Table 2. The cpu time of the new procedure includes the times for gridding all the data, resolving the north and east deflection of the vertical components and computing gravity anomalies using (45). It is evident that the method described in this paper is more than 100 times faster than least-squares collocation in the two test areas. The method of least-squares collocation needs a large amount of computer time because of the use of dense ERS-1/168-day data.

The gravity field in the area of the Reykjanes Ridge is shown in Fig. 5. An earlier field for the same area, constructed using least-squares collocation, was given by Hwang & Parsons (1995). A recent research cruise to the Reykjanes Ridge (cruise 87, RRS Charles Darwin) demonstrated that the earlier attempt accurately represented features with length-scales down to 20 km. Table 2 shows that the field, constructed using the modified spectral technique described in this paper, comes closer to matching the accuracy of least-squares collocation than the standard spectral method. The density of altimetry coverage has increased with the availability of the ERS-1/168-day data since the earlier attempt of Hwang & Parsons

Table 2. Comparison betweeen ship gravity and the satellite gravities derived from various methods.

(a) Reykjanes Ridge

method	std. dev. of diff. (mgals)	cpu time (seconds)	number of ship measurements
collocation	6.15	49613	95238
fft, this paper	7.05	470	95238
Sandwell et al., 1994	8.40	-	95238

(b) South Pacific

method	std. dev. of diff. (mgals)	cpu time (seconds)	number of ship measurements
collocation	3.70	68097	14713
fft, this paper	3.94	473	14713
Sandwell et al., 1994	4.05	-	14713

(1995). However, the latter field also incorporated ship gravity for the area. Where the ship gravity coverage is sparse, for example the southern part of the ridge, one can now have much greater confidence in the small-scale variability seen along-axis. A problem that remains to be solved is whether it is possible to adapt the techniques in this paper so that the gridded deflections of the vertical and ship gravity can be used together to calculate gravity anomalies. Where dense coverage of ship gravity exists over a sufficiently large area—this is increasingly a byproduct of high-resolution bathymetric surveys—it may be possible to combine the gravity spectrum derived from the deflection of the vertical as in (45), and a gravity spectrum derived from the ship gravity, in some optimal way. Elsewhere, it may be necessary to treat the satellite-derived gravity grid as point data, which are then mixed with the randomly distributed ship-gravity values to form a new gravity grid. In this approach, careful weighting of the two data types will be essential in obtaining a good combined field.

A colour shaded-relief map of the gravity field over part of the South Pacific is shown in Fig. 6. The spacing between adjacent altimeter ground tracks halves in going from the equator to latitudes of 60°. Also, the amplitudes of short-wavelength features are larger in the area of the Reykjanes Ridge than for the South Pacific area. The latter area provides a more stringent test, therefore, of the ability to resolve short-wavelength features. Because the gravity field for the South Pacific area would otherwise be dominated by longer-wavelength features, we have removed a reference field up to degree and order 10. The lineated gravity anomalies first noted by Haxby & Weissel (1986) are clearly visible in Fig. 6. These features are aligned with the direction of motion of the Pacific plate in a hot-spot frame of reference. Haxby & Weissel (1986) suggested that the gravity lineations reflect the development of small-scale convection from a convective instability occurring beneath the cooling lithospheric plate (Parsons & McKenzie 1978; Buck & Parmentier 1986). Alternative explanations—involving numerous mini-hotspots (Fleitout & Moriceau 1992) or lithospheric stretching of the Pacific plate (Sandwell *et al.* 1995)—have since been proposed. The present gravity field is able to resolve many more seamounts than previously. There are several seamount chains, also aligned with the direction of motion of the Pacific plate. The lineated gravity anomalies, which have wavelengths across-strike of 150–200 km, seem to develop and reach full amplitude some distance away from the East Pacific Rise. However, there are some linear seamount chains closer to the ridge-axis, and it is not clear whether there is any connection between the lineated gravity anomalies and variations along the ridge. The East Pacific Rise can also be clearly seen in Fig. 6, despite the fact that the direction of illumination was chosen to enhance the gravity lineations. Fast-spreading ridges are characterized by a small gravity high of almost constant amplitude (e.g. Owens & Parsons 1994); the axial gravity high in Fig. 6 appears continuous over several hundred kilometres along the axis.

The density of altimeter coverage will increase yet further as data from new satellite missions become available—for example ERS-2, SALT, SPOT-3 and MOS-2 (Seeber 1993). ERS-1 has now completed a second 168-day cycle; when this is fully available the ERS-1/168-day data set will be twice as dense as that used in this study, i.e. equivalent to the coverage of Geosat/GM. The procedure described in this paper provides a rapid means of updating the global marine gravity field as new sea-surface height measurements accumulate. The modified spectral technique used retains the speed of previous spectral methods, but features similar to those used in least-squares collocation are included, resulting in gravity anomalies comparable in data quality to those derived by the latter technique. At present, where the area of study is relatively small, it may still be desirable to use least-squares collocation. Some of the steps in the new procedure, for example the fast method of gridding the along-track deflections of the vertical and the method of resolving the north and east components, may have additional applications. For example, the technique of fast collocation (Bottoni & Arzaghi, 1993) requires the data to be on a grid, so that the covariance matrix of the data will be in Toeplitz form and can be quickly inverted. Because least-squares collocation gives the most accurate result, it may be possible to combine fast collocation with the efficient gridding of deflections of the vertical to retain the accuracy of general least-squares collocation without requiring a large amount of computer time.

ACKNOWLEDGMENTS

The ideas in this paper were conceived when the first author was a postdoctoral researcher in the Department of Earth Sciences, Oxford University, supported by a grant from Amoco Exploration (UK). Subsequent research was also supported by the National Science Council of the Republic of China, under contract NSC84-2211-E-009-039. We are grateful to

Jenny Collier for her help in processing the ERS-1 altimeter data.

REFERENCES

Bendat, J.S. & Piersol, A.G., 1993. *Engineering Applications of Correlation and Spectral Analysis,* 2nd edn, John Wiley & Sons, Inc., New York, NY.

Bottoni, G.P. & Arzaghi, R., 1993. Fast collocation, *Manuscripta geodaetica,* **67,** 119–126.

Buck, W.R. & Parmentier, E.M., 1986. Convection beneath young oceanic lithosphere; implications for thermal structure and gravity. *J. geophys. Res.,* **91,** 1961–1974.

Carlowicz, M., 1995. New map of seafloor mirrors surface, *EOS, Trans. Am. geophys. Un.,* **76,** 441–442.

de Boor, C., 1978. *A Practical Guide to Splines,* Springer-Verlag, New York, NY.

Fleitout, L. & Moriceau, C., 1992. Short wavelength geoid and bathymetry and the convective pattern beneath the Pacific plate, *Geophys. J. Int.,* **110,** 6–28.

Haxby, W.F. & Weissel, J.K., 1986. Evidence for small-scale mantle convection from Seasat altimeter data, *J. geophys. Res.,* **91,** 3507–3520.

Haxby, W.F., Karner, G.D., LaBrecque, J.L. & Weissel, J.K., 1983. Digital images of combined oceanic and continental data sets and their use in tectonic studies, *EOS, Trans. Am. geophys. Un.,* **64,** 995–1004.

Heiskanen, W. & Moritz, H., 1985. *Physical geodesy,* W. H. Freeman & Co., San Francisco, CA, 1967, reprint, Institute of Physical Geodesy, Tech. University of Graz, Austria.

Hwang, C. & Parsons, B., 1995. Gravity anomalies derived from Seasat, Geosat, ERS-1 and TOPEX/POSEIDON altimetry and ship gravity: a case study over the Reykjanes Ridge, *Geophys. J. Int.,* **122,** 551–568.

Kaula, W.M., 1966. *Theory of Satellite Geodesy,* Blaisdell Co., London.

Koch, K.R., 1987. *Parameter Estimation and Hypothesis Testing in Linear Models,* Springer-Verlag, New York, NY.

Lebedev, N.N., 1972. *Special Functions and their Applications,* Dover Publications, Inc., New York, NY.

McAdoo, D.C. & Marks, K., 1992. Gravity over the southern ocean from Geosat data, *J. geophys. Res.,* **97,** 3247–3260.

Mesko, A.M., 1984. *Digital Filtering: Applications in Geophysical Exploration for Oil,* Akademiai Kiado, Budapest.

Moritz, H., 1980. *Advanced Physical Geodesy,* Abacus Press, Karlsruhe.

Owens, R. & Parsons, B., 1994. Gravity fields over mid-ocean ridges from Geosat GM data: variations as a function of spreading rate, *Geophys. Res. Lett.,* **21,** 2837–2840.

Parsons, B. & McKenzie, D., 1978. Mantle convection and the thermal structure of the plates, *J. geophys. Res.,* **83,** 4485–4496.

Rapp, R.H., Wang, Y.M. & Pavlis, N., 1991. *The Ohio State 1991 geopotential and sea surface topography harmonic coefficient models,* Rep. 410, Dept. of Geod. Sci. and Surv., Ohio State University, Columbus, Ohio.

Sandwell, D.T., 1984. A detailed view of the South Pacific geoid form satellite altimetry, *J. geophys. Res.,* **89,** 1089–1104.

Sandwell, D.T., 1992. Antarctic marine gravity field from high-density satellite altimetry, *Geophys. J. Int.,* **109,** 437–448.

Sandwell, D.T., Yale, M.M. & Smith, W.H., 1994. ERS-1 Geodetic mission reveals detailed tectonic structures, *EOS, Trans. Am. geophys. Un.,* **75,** 44 (supplement).

Sandwell, D.T., Winterer, E.I., Mammerickx, J., Duncan, R.A., Lynch, M.A., Levitt, D.A. & Johnson, C.L., 1995. Evidence for diffuse extension of the Pacific plate from Puka-puka ridges and cross-grain gravity lineations, *J. geophys. Res.,* **100,** 15 087–15 099.

Schwarz, K.P., Sideris, M.G. & Forsberg, R., 1990. The use of FFT techniques in physical geodesy, *Geophys. J. Int.,* **100,** 485–514.

Seeber, G., 1993. *Satellite geodesy: foundations, methods, and applications,* Walter de Gruyter, New York, NY.

Sideris, M.G. & Li, Y.C., 1993. Gravity field convolutions without windowing and edge effects, *Bull. Géodésique,* **67,** 107–118.

Smith, W.H.F. & Wessel, P., 1990. Gridding with continuous curvature splines in tension, *Geophysics,* **55,** 293–305.

Vassiliou, A.A., 1986. *Numerical techniques for processing airborne gradiometer data,* UCSE Rep. No. 20017, Division of Surveying Engineering, The University of Calgary, Calgary, Canada.

Wang, Y.M., 1993. On the optimal combination of potential coefficient model with terrestrial gravity for FFT geoid computation, *Manuscripta geodaetica,* **18,** 406–416.

Wessel, P. & Smith, W.H., 1991. Free software helps map and display data, *EOS, Trans. Am. geophys. Un.,* **72,** 441–446.

APPENDIX A: GRAVITY DEFLECTION-OF-THE-VERTICAL CONVERSION IN THE CASE OF A SINGLE SATELLITE WITH A HIGH INCLINATION ANGLE

Reduced along-track deflection of the vertical

Here we will investigate a numerical problem when applying (27) in the case of data from one satellite and seek an improved procedure. For a satellite such as ERS-1, whose orbital inclination is about 98°, the term $\sin\alpha_a$ becomes very small and will create a numerical problem for the east component η as determined from (27). The problem can best be examined in terms of covariance propagation. Assuming that the ascending and descending deflections of the vertical are uncorrelated and their error variances are of the same magnitude, we can derive the error variances of ξ and η as

$$\sigma_\xi^2 = \frac{1}{4\cos^2\alpha_a}(\sigma_a^2+\sigma_d^2) = \frac{\sigma_a^2}{2\cos^2\alpha_a},$$
$$\sigma_\eta^2 = \frac{1}{4\sin^2\alpha_a}(\sigma_a^2+\sigma_d^2) = \frac{\sigma_a^2}{2\sin^2\alpha_a}. \tag{A1}$$

Thus, the ratio of the two error variances is

$$\frac{\sigma_\eta^2}{\sigma_\xi^2} = \frac{\cos^2\alpha_a}{\sin^2\alpha_a}. \tag{A2}$$

If, for example, $\alpha_a = 8°$, then σ_η^2 is 50 times larger than σ_ξ^2. Thus the noise of the east component is greatly amplified to the extent that any filter will not properly remove it. A similar situation occurs for the north component when α_a approaches 90° or when the satellite reaches its maximum absolute latitudes.

In view of this numerical problem, an improved procedure is suggested below. First, we obtain the reduced deflection of the vertical along a fixed azimuth α_0 (for the ascending deflection of the vertical) and $(\pi-\alpha_0)$ (for the descending deflection of the vertical) using (26):

$$\varepsilon_a^0 = \xi\cos\alpha_0 + \eta\sin\alpha_0$$
$$= \frac{1}{\sin 2\alpha_a}[\varepsilon_a\sin(\alpha_0+\alpha_a) + \varepsilon_d\sin(\alpha_0-\alpha_a)],$$
$$\varepsilon_d^0 = \xi\cos(\pi-\alpha_0) + \eta\sin(\pi-\alpha_0) \tag{A3}$$
$$= \frac{1}{\sin 2\alpha_a}[\varepsilon_a\sin(\alpha_0-\alpha_a) + \varepsilon_d\sin(\alpha_0+\alpha_a)].$$

The value α_0 should be chosen at the geographic centre of the work area. The reduced deflections of the vertical from the transformation in (A3) are then functions of two variables, like ξ and η, and can be operated on in the same way. The error variances of ε_a^0 and ε_d^0 are

$$\sigma_{a_0}^2 = \frac{1}{\sin^2 2\alpha_a}[\sigma_a^2 \sin^2(\alpha_0 + \alpha_a) + \sigma_d^2 \sin^2(\alpha_0 - \alpha_a)],$$
$$\sigma_{d_0}^2 = \frac{1}{\sin^2 2\alpha_a}[\sigma_a^2 \sin^2(\alpha_0 - \alpha_a) + \sigma_d^2 \sin^2(\alpha_0 + \alpha_a)]. \quad \text{(A4)}$$

If $\sigma_a \approx \sigma_d$, and $\alpha_0 \approx \alpha_a$, we will have

$$\sigma_{a_0}^2 \approx \sigma_a^2,$$
$$\sigma_{d_0}^2 \approx \sigma_d^2. \quad \text{(A5)}$$

Therefore the error variances of ε_a^0 and ε_d^0 are almost identical to those of ε_a and ε_d, and none of the two has increased noise. At this stage, we can filter ε_a^0 and ε_d^0 using an optimal filter (see below). Furthermore, by (27) we have

$$\xi = \frac{1}{2\cos\alpha_0}(\varepsilon_a^0 - \varepsilon_d^0),$$
$$\eta = \frac{1}{2\sin\alpha_0}(\varepsilon_a^0 + \varepsilon_d^0). \quad \text{(A6)}$$

Fourier transforming the above equation and substituting into (9) gives

$$\Delta G = \frac{i\gamma}{2q}\left[\frac{u}{\sin\alpha_0}(E_a^0 + E_d^0) + \frac{v}{\cos\alpha_0}(E_a^0 - E_d^0)\right], \quad \text{(A7)}$$

where E_a^0 and E_d^0 are the FTs of ε_a^0 and ε_d^0, respectively.

Wiener filter

The reduced components of the deflection of the vertical given by (A3) can be filtered by a Wiener filter. To this end we have to estimate the noise spectra of the reduced deflection of the vertical. Assuming that the reduced deflections of the vertical contain noise levels n and m, we can write

$$\varepsilon_a^0 = \xi\cos\alpha_0 + \eta\sin\alpha_0 + n \quad \text{(A8)}$$

and

$$\varepsilon_d^0 = -\xi\cos\alpha_0 + \eta\sin\alpha_0 + m. \quad \text{(A9)}$$

Assuming that the signals and noise are uncorrelated, we can Fourier transform both sides of (A8) and (A9), and use the relationship in (8), to obtain the spectral density functions of the two reduced components of the deflection of the vertical:

$$S_{aa} = \frac{\Delta G^* \Delta G}{\gamma^2 q^2}(u\sin\alpha_0 + v\cos\alpha_0)^2 + S_{nn}, \quad \text{(A10)}$$

$$S_{dd} = \frac{\Delta G^* \Delta G}{\gamma^2 q^2}(u\sin\alpha_0 - v\cos\alpha_0)^2 + S_{mm}, \quad \text{(A11)}$$

$$S_{ad} = \frac{\Delta G^* \Delta G}{\gamma^2 q^2}(u^2\sin^2\alpha_0 - v^2\cos^2\alpha_0), \quad \text{(A12)}$$

where S_{aa} and S_{dd} are the auto-spectral density functions of the reduced ascending and descending components of the deflection of the vertical, respectively, S_{ad} is the cross-spectral density function of the two components, and S_{nn} and S_{mm} are the auto-spectral density functions of the noise. On moving S_{nn} and S_{mm} to the left sides of (A10) and (A11) and dividing the resulting equations by (A12), we obtain

$$S_{nn} = S_{aa} - \frac{(u\sin\alpha_0 + v\cos\alpha_0)^2}{u^2\sin^2\alpha_0 - v^2\cos^2\alpha_0}S_{ad}, \quad \text{(A13)}$$

$$S_{mm} = S_{dd} - \frac{(u\sin\alpha_0 - v\cos\alpha_0)^2}{u^2\sin^2\alpha_0 - v^2\cos^2\alpha_0}S_{ad}. \quad \text{(A14)}$$

To obtain circularly symmetric and smooth spectral density functions of the noises we can employ azimuthal smoothing, defined by

$$\bar{S}_{nn}(q) = \frac{1}{2\pi}\int_0^{2\pi} S_{nn}(q\cos\psi, q\sin\psi)\,d\psi, \quad \text{(A15)}$$

$$\bar{S}_{mm}(q) = \frac{1}{2\pi}\int_0^{2\pi} S_{mm}(q\cos\psi, q\sin\psi)\,d\psi, \quad \text{(A16)}$$

where $q\cos\psi = u$, and $q\sin\psi = v$. We can also use this procedure to derive circularly symmetric forms for S_{aa} and S_{dd}. Fig. A1 compares the spectral density functions of signal and noise for the reduced ascending component of the deflection of the vertical from the ERS-/168-day and ERS-1/35-day data over the Reykjanes Ridge. The latter are averaged from 18 cycles of data. The noise of the ERS-1/168-day deflections of the vertical is clearly larger than that for ERS-1/35-day data. At lower frequencies, the signal spectra from ERS-1/35-day and ERS-1/Gm agree very well.

Using the estimated noise spectra, the Wiener filters for ε_a^0 and ε_d^0 can be calculated by

$$\Phi_a(q) = \frac{\bar{S}_{aa}(q) - \bar{S}_{nn}(q)}{\bar{S}_{aa}(q)}, \quad \text{(A17)}$$

$$\Phi_d(q) = \frac{\bar{S}_{dd}(q) - \bar{S}_{mm}(q)}{S_{dd}(q)}. \quad \text{(A18)}$$

To obtain smooth Wiener filters and to investigate the filter widths, we least-squares fit the values as computed from (A17) and (A18) by a Gaussian function of the form $\exp(-\pi d^2 q^2)$, where d is the filter width. Note that the inverse Fourier transform of $\exp(-\pi d^2 q^2)$ is $[\exp(-\pi x^2/d^2)]/d$ which is the Gaussian filter in the space domain. The filtered deflections of the vertical in the frequency domain are

$$\tilde{E}_a^0(u, v) = \Phi_a(q)E_a^0, \quad \text{(A19)}$$

$$\tilde{E}_d^0(u, v) = \Phi_d(q)E_d^0. \quad \text{(A20)}$$

The raw deflection of the vertical in (A7) should be replaced by the filtered deflection of the vertical for the computation of gravity anomalies. Fig. A2 compares Wiener filters for the deflection-of-the-vertical from ERS-1/35-day and ERS-1/168-day data. The filter widths as determined by the Gaussian function fits for ERS-1/35-day ascending and descending deflections of the vertical are 23.89 and 27.14 km, respectively, while for ERS-1/168-day data the numbers are 9.14 and 8.57 km. Based on these numbers and Fig. A2, the estimated 2-D resolutions of ERS-1/35-day data and ERS-1/168-day data are 3–4 cycle degree^{-1} and 11–12 cycle degree^{-1}, respectively.

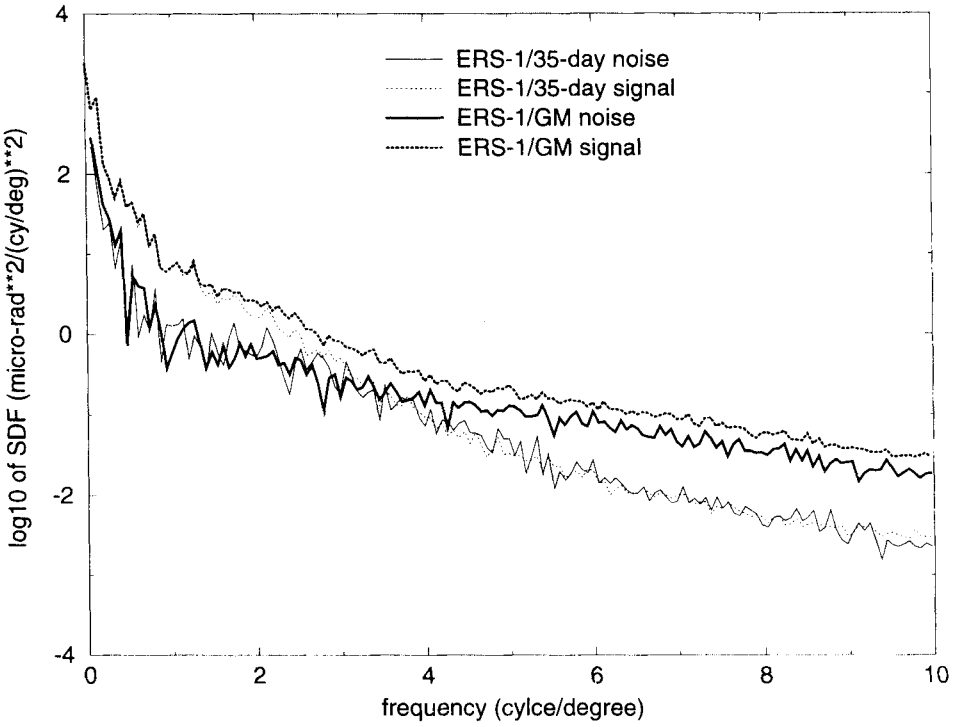

Figure A1. Spectral density functions (SDF) of the signal and noise of the ascending deflection of the vertical from ERS-1/35-day and ERS-1/168-day data over the Reykjanes Ridge.

APPENDIX B: FOURIER TRANSFORMS OF TRUNCATED KERNEL FUNCTIONS IN ANALYTICAL FORM

Analytical expressions of the truncated kernel functions $\bar{l}_\xi$ and $\bar{l}_\eta$ will be derived here. The function $w(x, y)$ in (41) can be approximated by a complex Fourier series,

$$w(x,y) = \lim_{T\to\infty} \sum_{m=-\infty}^{\infty} \sum_{n=-\infty}^{\infty} c_{mn} \exp\left[i\pi\left(\frac{m}{T}x + \frac{n}{T}y\right)\right], \tag{B1}$$

where c_{mn} are the complex Fourier coefficients. By the change of variables

$$\bar{x} = \frac{\pi x}{T}, \qquad \bar{y} = \frac{\pi y}{T}, \tag{B2}$$

we obtain c_{mn} by

$$c_{mn} = \frac{1}{4\pi^2} \int_{-\pi}^{\pi}\int_{-\pi}^{\pi} \bar{w}(\bar{x},\bar{y}) \exp[-i(m\bar{x} + n\bar{y})]\, d\bar{x}\, d\bar{y}, \tag{B3}$$

where

$$\bar{w}(\bar{x},\bar{y}) = \begin{cases} 1, & \bar{r} = \sqrt{\bar{x}+\bar{y}^2} \le \dfrac{\pi}{T}R, \\ 0, & \bar{r} > \dfrac{\pi}{T}R. \end{cases} \tag{B4}$$

By the definition of the Hankel transform (Mesko 1984) and using the polar coordinates

$$\begin{aligned} &\bar{x} = \bar{r}\cos\theta, \qquad \bar{y} = \bar{r}\sin\theta, \\ &m = k\cos\psi, \qquad n = k\sin\psi, \qquad k = \sqrt{m^2+n^2}, \end{aligned} \tag{B5}$$

we have

$$\begin{aligned} c_{mn} &= \frac{1}{4\pi^2} \int_{\bar{r}=0}^{(\pi/T)R} \bar{r}\, d\bar{r} \int_{\theta=-\pi}^{\pi} \exp[-ik\bar{r}\cos(\theta-\psi)]\, d\theta \\ &= \frac{1}{2\pi} \int_{\bar{r}=0}^{(\pi/T)R} \bar{r} J_0(k\bar{r})\, d\bar{r}. \end{aligned} \tag{B6}$$

Using the formula for Bessel functions of integral order (Lebedev 1972, p. 100),

$$\frac{d}{dx}[x^n J_n(x)] = x^n J_{n-1}(x), \tag{B7}$$

with $x = kr$ we have

$$\frac{d}{dr}[rJ_1(kr)] = krJ_0(kr). \tag{B8}$$

Replacing the variable r by $\bar{r}$ and integrating (B8), we obtain:

$$\int_0^{(\pi/T)R} \bar{r}J_0(k\bar{r})\, d\bar{r} = \frac{1}{k}\bar{r}J_1(k\bar{r})\Big|_{\bar{r}=0}^{\bar{r}=(\pi/T)R} = \frac{\pi R}{Tk} J_1\left(\frac{k\pi}{T}R\right). \tag{B9}$$

Thus,

$$c_{mn} = \frac{R}{2Tk} J_1\left(\frac{k\pi}{T}R\right). \tag{B10}$$

With (B10), the FTs of $\bar{l}_\xi$ and $\bar{l}_\eta$ are

$$\begin{Bmatrix} \bar{L}_\xi \\ \bar{L}_\eta \end{Bmatrix} = \sum_{m=-\infty}^{\infty} \sum_{n=-\infty}^{\infty} c_{mn} \begin{Bmatrix} \mathcal{F}\left(l_\xi \exp\left[\dfrac{i\pi}{T}(mx+ny)\right]\right) \\ \mathcal{F}\left(l_\eta \exp\left[\dfrac{i\pi}{T}(mx+ny)\right]\right) \end{Bmatrix} \tag{B11}$$

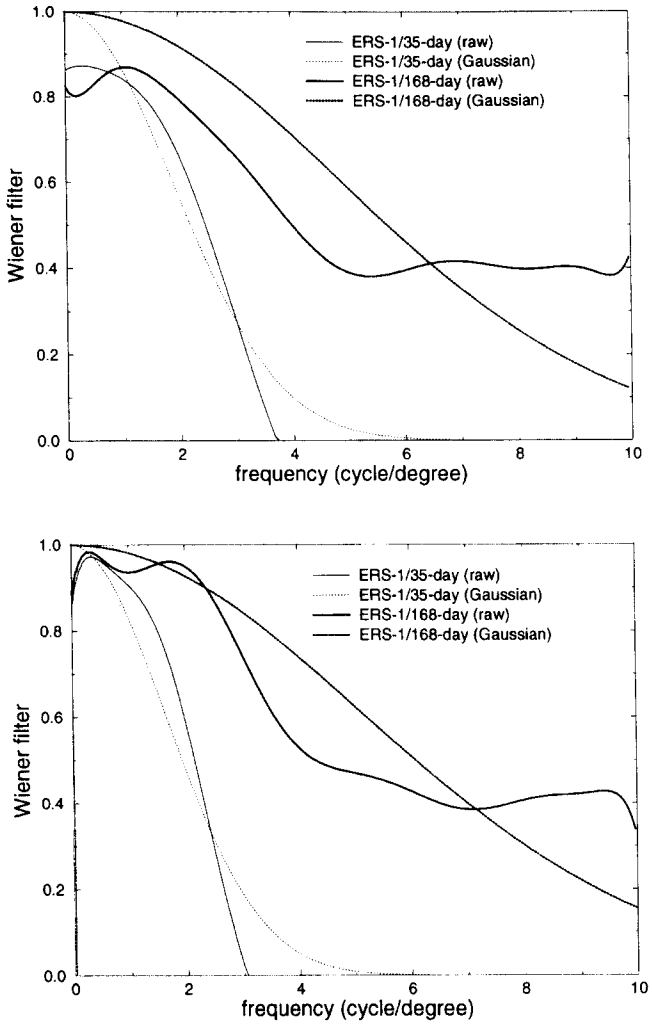

Figure A2. Gaussian-fitted Wiener filters for along-track deflection of the vertical from ERS-1/35-day and ERS-1/168-day altimetry over the Reykjanes Ridge. The top figure is for the ascending tracks and the bottom one is for the descending tracks.

Using the theorem of frequency shift, we have

$$\mathcal{F}\left(\begin{Bmatrix} l_\xi \\ l_\eta \end{Bmatrix} \exp\left[\frac{i\pi}{T}(mx+ny)\right]\right) = \begin{Bmatrix} L_\xi\left(u-\frac{m}{2T}, v-\frac{n}{2T}\right) \\ L_\eta\left(u-\frac{m}{2T}, v-\frac{n}{2T}\right) \end{Bmatrix}$$

$$= \frac{-2\pi i}{\sqrt{\left(u-\frac{m}{2T}\right)^2+\left(v-\frac{n}{2T}\right)^2}} \times \begin{Bmatrix} \left(v-\frac{n}{2T}\right) \\ \left(u-\frac{m}{2T}\right) \end{Bmatrix}. \quad \text{(B12)}$$

In conclusion,

$$\begin{Bmatrix} \bar{L}_\xi(u,v) \\ \bar{L}_\eta(u,v) \end{Bmatrix} = \frac{-2\pi R i}{D} \sum_{m=-\infty}^{\infty} \sum_{n=-\infty}^{\infty} \frac{J_1\left(\frac{2\pi\sqrt{m^2+n^2}}{D}R\right)}{\sqrt{m^2+n^2}} \times \frac{1}{\sqrt{\left(u-\frac{m}{D}\right)^2+\left(v-\frac{n}{D}\right)^2}} \begin{Bmatrix} \left(v-\frac{n}{D}\right) \\ \left(u-\frac{m}{D}\right) \end{Bmatrix}, \quad \text{(B13)}$$

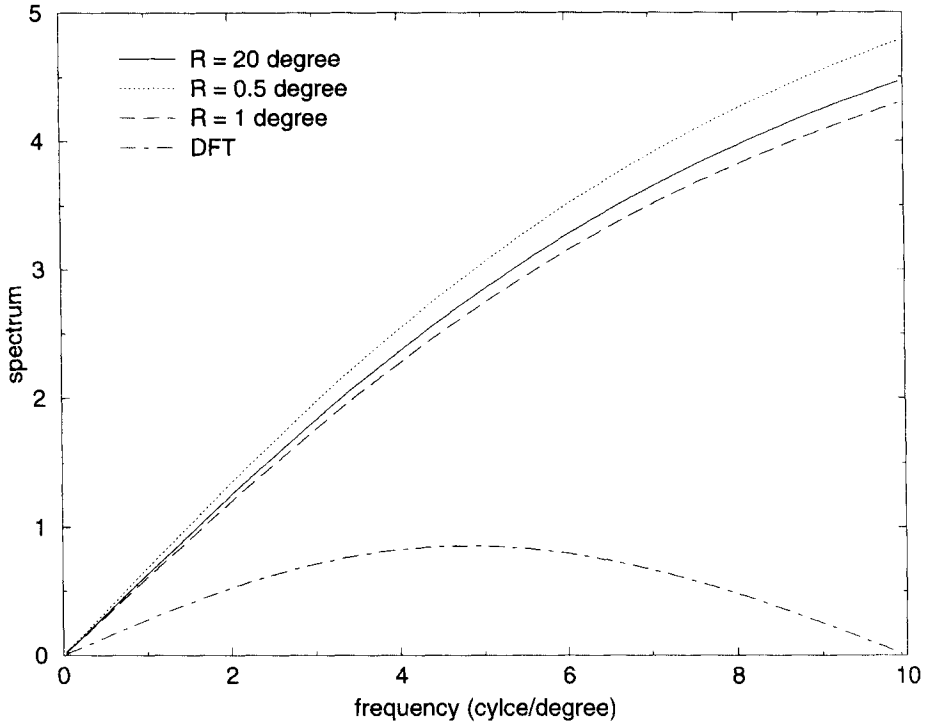

Figure B1. The spectra of the truncated kernel function $\bar{l}_\xi$ along the u direction for various radii R (note: 1° is equivalent to 111 km). The expansion degree in the Fourier series is 300. The frequency along the v direction is fixed at 0.04 cycle degree^{-1}. The spectrum with $R = 20°$ is equivalent to the spectrum of the original kernel function.

where $D = 2T$. For a numerical computation, it is noted that

$$\lim_{k\to 0}\frac{J_1\left(\frac{2\pi k}{D}R\right)}{k} = \lim_{k\to 0}\frac{\partial}{\partial k}\left(J_1\left(\frac{2\pi k}{D}R\right)\right)$$
$$= \frac{\pi R}{D}(J_0(0) - J_2(0))$$
$$= \frac{\pi R}{D}. \tag{B14}$$

When $u - (m/D) = 0$ and $v - (n/D) = 0$, we have

$$\frac{1}{\sqrt{\left(u-\frac{m}{D}\right)^2+\left(v-\frac{n}{D}\right)^2}}\begin{Bmatrix}\left(v-\frac{n}{D}\right)\\ \left(u-\frac{m}{D}\right)\end{Bmatrix} = \begin{Bmatrix}1\\1\end{Bmatrix}. \tag{B15}$$

To verify the formula given in (B13), one may choose a large R value so that $\bar{L}_\xi \approx L_\xi$ and $\bar{L}_\eta \approx L_\eta$ and the exact values of $\bar{L}_\xi$ and $\bar{L}_\eta$ will be known. Fig. B1 shows the spectra of $\bar{l}_\xi$ and $\bar{l}_\eta$, which are the imaginary parts of (B13). Using an expansion degree to $m = n = \pm 300$ it is found that with $R = 20°$ $\bar{L}_\xi$ and $\bar{L}_\eta$ are practically identical to L_ξ and L_η with a relative difference below 10^{-5}. Use of degrees higher than 300 reduces the difference only marginally, thus we decided to use $m = n = \pm 300$ for all the computations described in this paper. Also shown in Fig. B1 are the discrete Fourier transforms (DFT) of l_ξ, l_η, which exhibit large deviations from the theoretical values, especially at high frequencies. This implies that we may not obtain correct spectra of $\bar{l}_\xi$ and $\bar{l}_\eta$ by DFT.

For practical applications, it would be extremely time-consuming to compute $\bar{L}_\xi$ and $\bar{L}_\eta$ on a point-by-point basis. This problem can be overcome by computing $\bar{L}_\xi$ and $\bar{L}_\eta$ on a grid, and interpolating the required value from the grid. Experiments show that for $R = 0.5°, 1°, 2°$, a grid interval of 0.1 cycle degree^{-1} for u, v, and a bicubic spline interpolation yield values identical to those computed by (B13). For the current altimeter data density, a maximum frequency of 30 cycle degree^{-1}, equivalent to a data spacing of 1′, is sufficient for most uses. Furthermore, the following relationships will help to save storage space and computer time:

$$\bar{L}_\eta(-u, \pm v) = -\bar{L}_\eta(u, \pm v),$$
$$\bar{L}_\xi(u, v) = \bar{L}_\eta(v, u), \tag{B16}$$
$$\bar{L}_\eta(u, v) = \bar{L}_\eta(u, -v).$$